Cummings et al., http://www.jcb.org/cgi/content/full/jcb.201510065/DC1

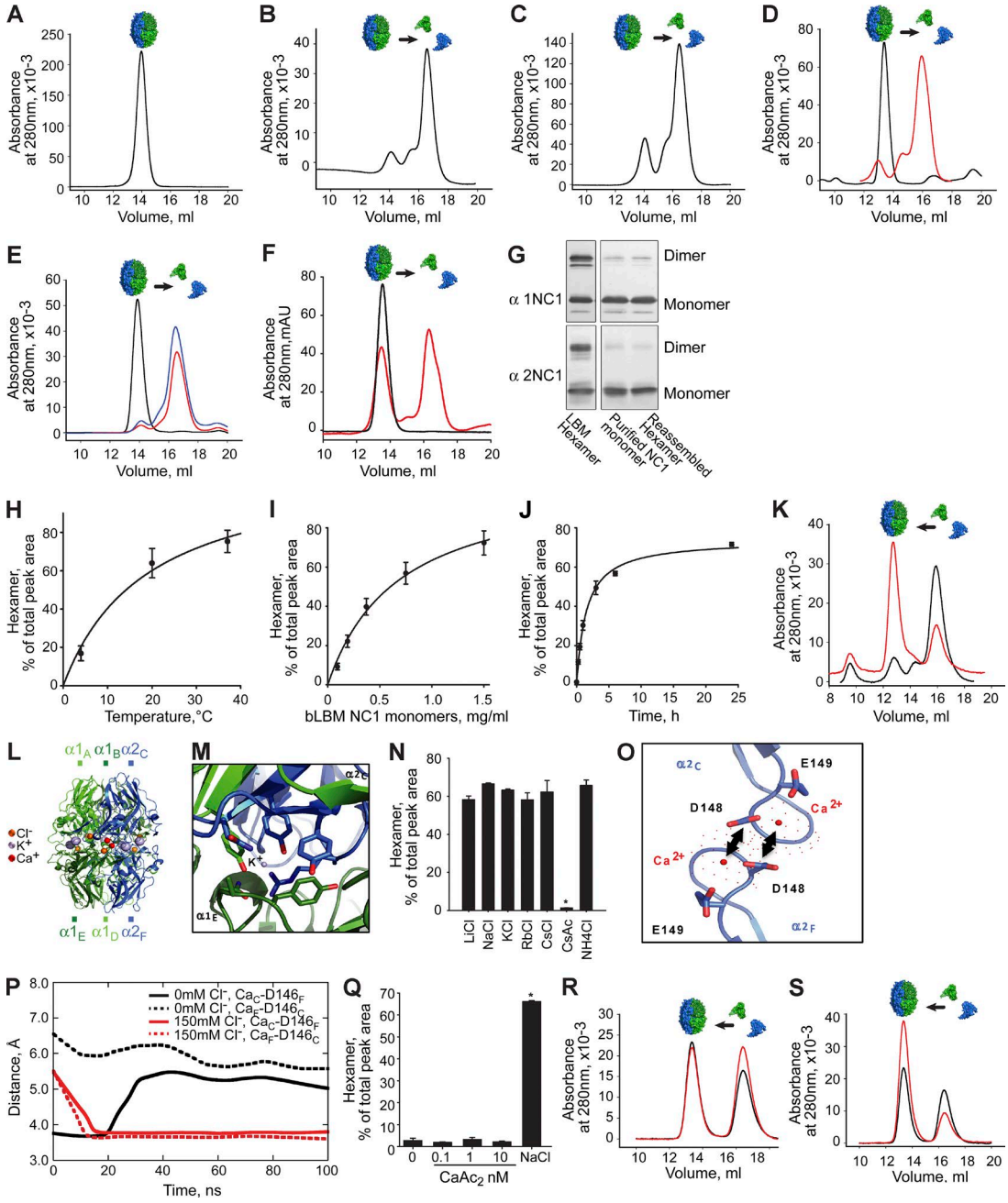

Figure S1. **Chloride is required for hexamer assembly.** (A–C) SEC profiles of native LBM NC1 hexamer in TBS (A) and LBM hexamer after dissociation in 6 M guanidine-HCl (B) or 8 M urea (C), causing loss of 14 ml hexamer peak and formation of 16.3 ml monomer peak. (D) Uncross-linked PFHR9 NC1 hexamers dissociate in TrisAc (red line) but not in TBS (black line). (E) Uncross-linked PFHR9 NC1 hexamers are stable in PBS (black line) but dissociate in 10 mM phosphate buffer, pH 7.4, irrespective of whether KI (red line) or phloroglucinol (blue line) was used to inhibit cross-linking in culture. (F) LBM hexamers dissociate in 10 mM phosphate buffer (red line; black line, undissociated control LBM hexamers in TBS, pH 7.4). (G) Composition of reassembled hexamers from LBM NC1 monomers in Cl^-. Western blots developed using monoclonal antibodies to α1NC1 and α2NC1 domains. Vertical line denotes image boundary between distant lanes. Positions of NC1 monomers and cross-linked dimers are shown. (H–J) Characterizing hexamer reassembly with respect to incubation temperature (H), starting concentration of NC1 monomers (I), and incubation time (J). (K) Reassembly of PFHR9 NC1 hexamers triggered by Cl^- (red line) from NC1 monomers (black line). (L) Molecular model of NC1 hexamer with individual NC1 domains labeled. (M) Molecular modeling of K^+ ions within hexamer structure. (N) Effect of monovalent cations on LBM hexamer reassembly (100 mM, Cl^- salts). CsAc did not support reassembly in contrast with CsCl, demonstrating importance of Cl^-. (O) Molecular model of Ca^{2+} in hexamer (α2 NC1) interacting with E^{149} and D^{148}. (P) MD simulations of distances between Ca^{2+} ions and the carboxyl carbon of aspartic acid residues. (Q) $CaAc_2$ alone does not induce hexamer assembly from 0.1 to 10 mM. (R) Cl^--dependent assembly occurs equally well in TBS alone (black line) or with 0.2 mM EDTA (red line). (S) Ca^{2+} may potentiate Cl^- activity because the addition of 1 mM $CaCl_2$ in 100 NaCl (red line) appeared to enhance hexamer formation over 100 mM NaCl alone (black line). *, $P < 0.01$.

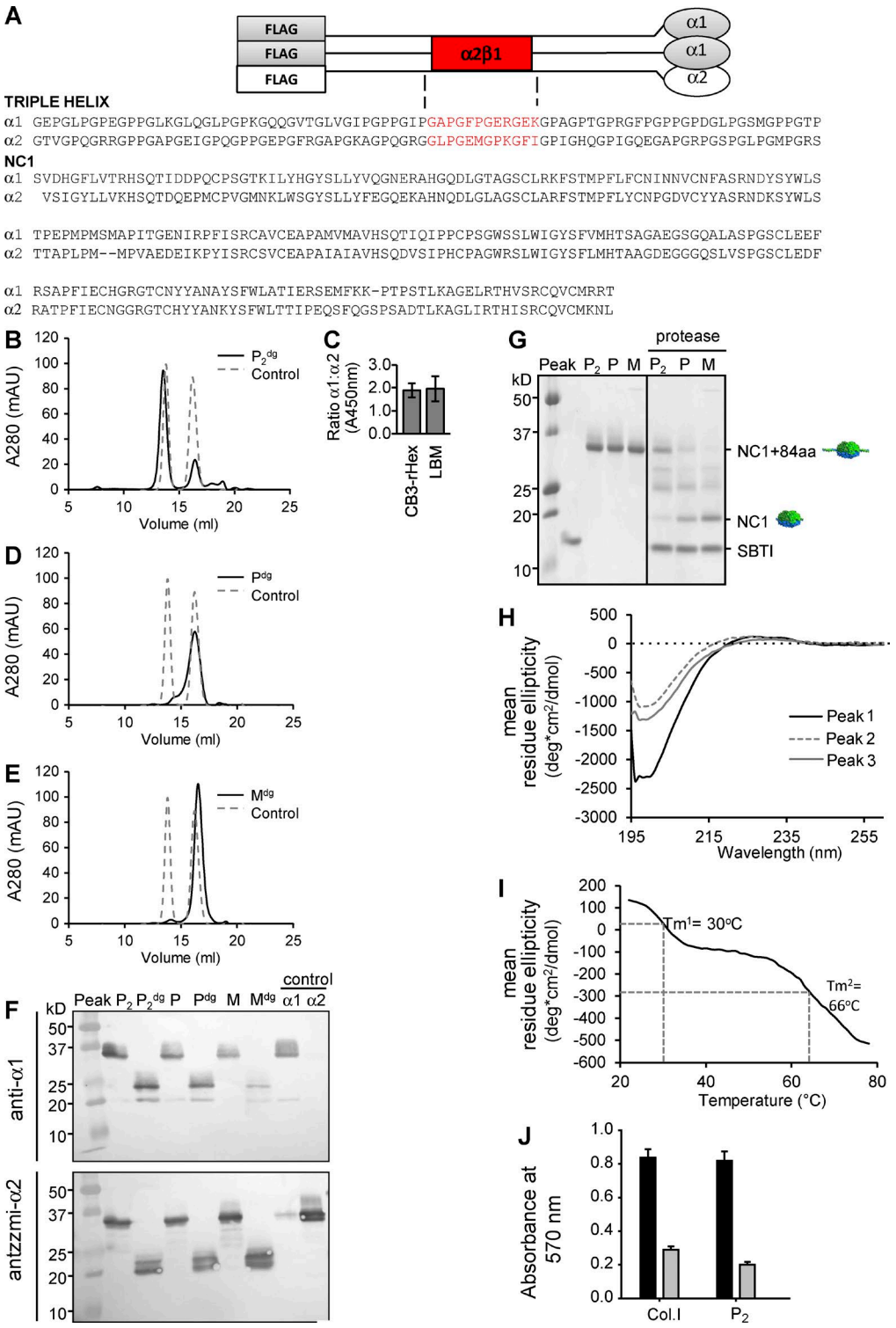

Figure S2. **Design and characterization of recombinant protomer (r-Prot).** (A) Schematic of heterotrimeric r-Prot containing integrin α2β1 binding site and N-terminal FLAG tag for purification. Primary aa sequence shown with red text identifying the engineered α2β1 integrin binding site. (B) SEC profile of P_2 samples after collagenase treatment (P_2^{dg}). Control sample (dashed line) contained mixture of NC1 hexamers isolated from LBM and recombinant α2 NC1 monomers. (C) ELISA analyses of P_2 (CB3-rHex) using anti-α1 and -α2 monoclonal antibodies. LBM NC1 hexamers were control. (D and E) SEC profiles of P (P^{dg}) and M (M^{dg}), respectively, after collagenase treatment. Control (dashed line) is the same as B. (F) Western blot of SEC peaks and collagenase digest products, using anti-α1 and -α2 monoclonal antibodies. Unfractionated samples (SEC input) served as controls. (G) All three SEC peaks migrate as 35 kD monomers by SDS-PAGE. P_2 resisted trypsin and chymotrypsin proteolysis (NC1+84aa). Soybean trypsin inhibitor (SBTI) quenched reaction. (H and I) CD spectroscopy of SEC peaks (P_2, peak 1; P, peak 2; and M, peak 3). Helical content seen by negative ellipticity at 198 nm and positive ellipticity at 220–235 nm. (I) r-Prot thermal stability measured by CD. 30°C and 66°C transition point correspond to melting temperatures of helices and NC1 domains, respectively. (J) HT1080 cells adhesion to recombinant protomer dimer (P_2) is mediated by the integrin α2β1. Cell adhesion to wells coated with P_2 (black bar) was significantly inhibited by neutralizing monoclonal antibody to α2β1 integrin (gray bar). Collagen I, a known ligand for α2β1 integrin, has been used as a positive control.

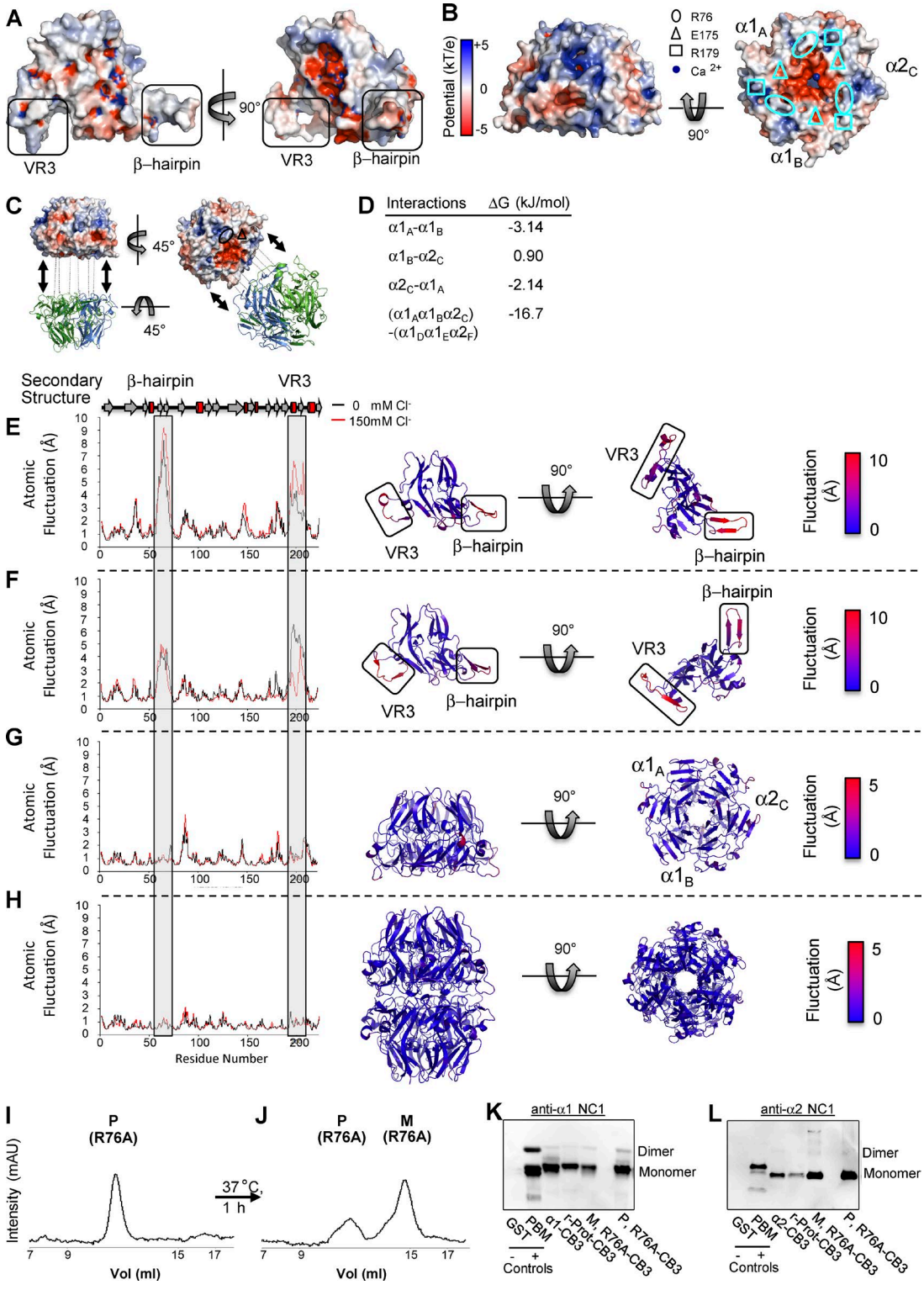

Figure S3. **Thermodynamic and mutational analysis of hexamer assembly.** (A) Protomer specificity is dictated by VR3 and β-hairpin interactions. Electrostatic surface potentials on the NC1 monomer van der Waals surface show the VR3 and β-hairpin regions are mostly charge neutral. (B) The trimer electrostatic surface potential shows that the interface is dominated by electro-negative potential in the center cavity that surrounds the calcium binding site, whereas R76, G175, and R179 comprise discrete charge pockets (units = Boltzman's constant [k] × temperature [298 K]/electron charge [q]). (C) Charged pockets are complementary in trimer–trimer association. (D) From nonlinear Poisson–Boltzmann calculations, salt has a favorable impact on a1A-a1B, a2C-a1A, and trimer–trimer association and a negative effect on a1B-a2C association. (E–H) Atomic fluctuations of the a1 monomer (E), a2 monomer (F), a112 trimer (F), and a112 hexamer (H) measured in 0 (black) and 150 mM Cl^- (red). β-Hairpin and VR3 regions denoted by gray filled boxes. For a112 trimer and hexamer system, the a1 A chain is depicted. Atomic fluctuations are projected onto representative structures (right). (I) R76A chimeras of both a1-CB3 and a2-CB3 constructs were expressed and combined to form P. (J) Above helical melting temperature, P samples with R76A mutations dissociated to monomeric chains by SEC. (K and L) Western blot analysis of R76A products, showing reactivity to α1 (K) and α2 (L) NC1 antibodies.

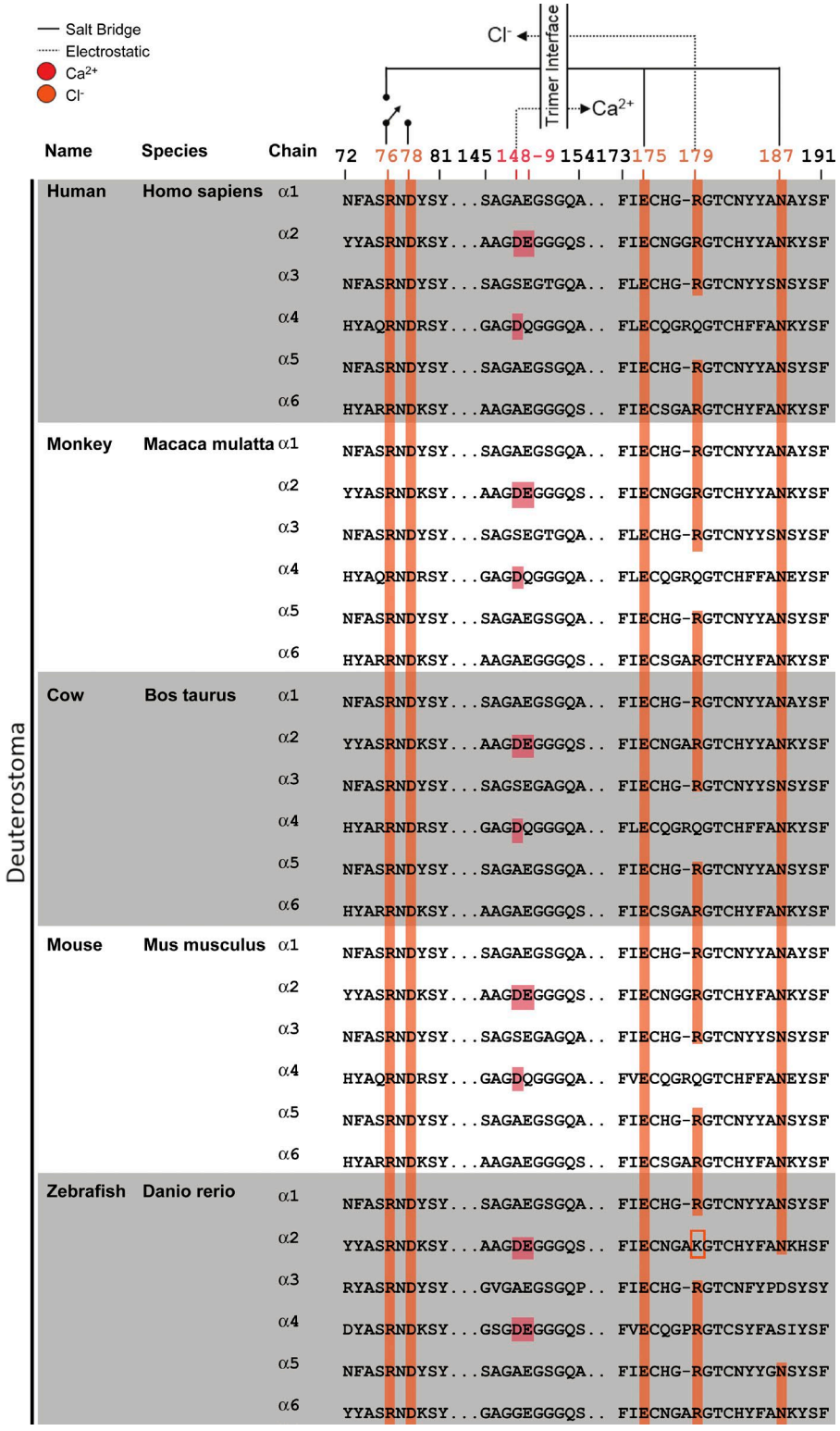

Figure S4. **Assembly Switch Motif is Present in α3-α6 Chains.** Multiple sequence alignment of α1-6 chains from human, monkey, cow, mouse, and zebrafish, with emphasis on putatively important assembly residues near the trimer–trimer interface.

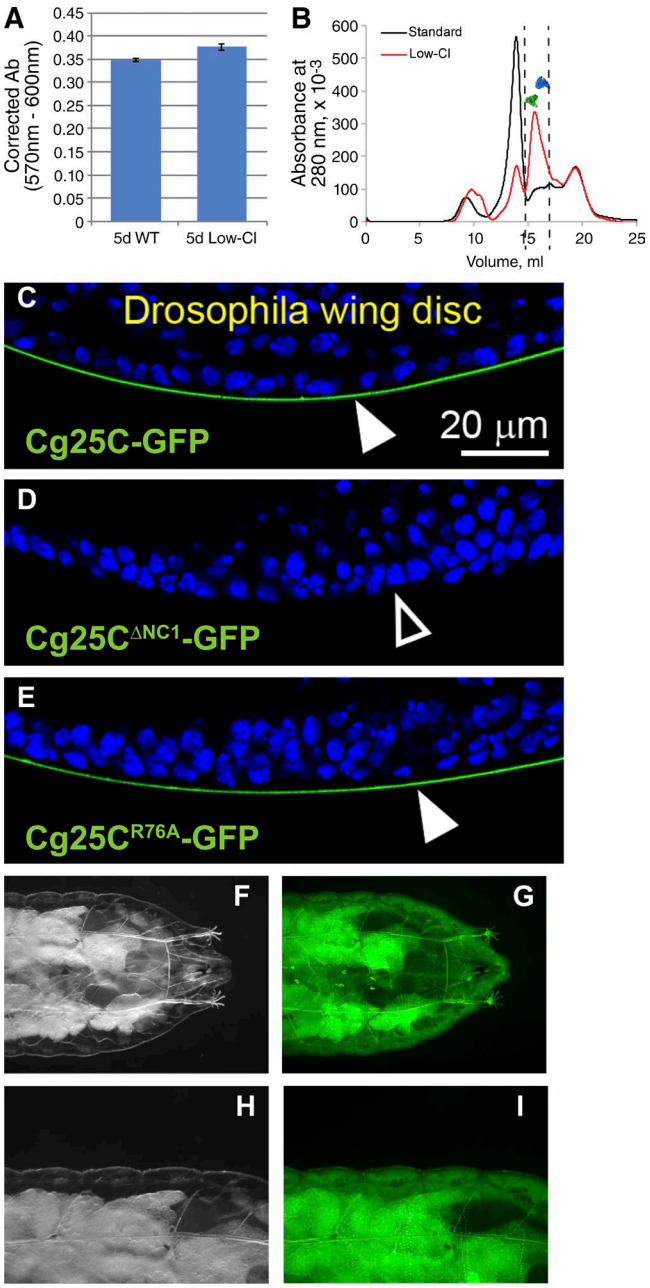

Figure S5. **NC1 domains are required for collagen IV network assembly.** (A) Cellular viability is not reduced in low-Cl conditions compared with standard conditions. Results shown from PrestoBlue assay. *n* = 12. (B) NC1 monomers from standard and low-Cl cultures were isolated via SEC. Samples analyzed after collagenase digestion and dialysis into 50 mM TrisAc. Dashed lines denote monomer fractions collected. (C–E) Confocal images of *Drosophila* wing imaginal disks dissected from larvae expressing C-terminally GFP-tagged Cg25C (C), Cg25CΔNC1 (D), and Cg25CR76A (E). Expression of the three constructs is driven in the fat body under control of Cg-GAL4. WT collagen IV (Cg25C-GFP) localizes to the BM (C), whereas Cg25CΔNC1-GFP does not incorporate into the BM in the presence of endogenous collagen IV (D). (F–I) Cg25CΔNC1-GFP expression products were detected in the larval body cavity, indicating that NC1 domains are required for assembling collagen IV into networks within BMs. H and I are enlarged images of F and G, respectively.

Table S1. **Comparison of interactions stabilizing monomer–monomer and trimer–trimer associations**

Interaction	Subunits	Salt bridges	Electrostatic	H-bonds	Total polar	Nonpolar	Total	Ratio (NP/P)
Trimer–trimer (end-to-end)	$a1_A$–$a1_D$	2	2	12	16	34	50	2.1
	$a1_A$–$a1_E$	0	0	2	2	23	25	11.5
	$a1_A$–$a2_F$	0	0	0	0	0	0	0
	$a1_B$–$a1_D$	0	0	3	3	21	24	7
	$a1_B$–$a1_E$	0	0	2	2	2	4	1
	$a1_B$–$a2_F$	2	2	9	13	39	52	3
	$a2_C$–$a1_D$	0	0	0	0	0	0	0
	$a2_C$–$a1_E$	2	2	12	16	44	60	2.8
	$a2_C$–$a2_F$	0	0	1	1	19	20	19
	Subtotal	6	6	41	53	182	235	3.4
	Density	0.45	0.45	3.1	4	13.8		3.5
Monomer–monomer (side-to-side)	$a1_A$–$a1_B$	1	0	15	16	81	97	5.1
	$a1_B$–$a2_C$	2	0	20	22	88	110	4
	$a2_C$–$a1_A$	1	0	17	18	83	101	4.6
	Subtotal	4	0	49	53	252	305	4.8
	Density	0.19	0	3.1	3.3	16.2		4.9

Enumeration of the modeled noncovalent interactions present between NC1 domains as well as between NC1 trimers, using the LIGPLOT+ algorithm (Wallace et al., 1995). NP, nonpolar; P, polar.

Table S2. **Low-Cl media composition**

Component	Catalog number	Final concentration	Molecular mass	mg/liter
		mM	*g/mol*	
Neutral aa				
Glycine	G7126	0.4	75.07	30.0
L-Arginine	A8094	0.4	174.2	69.7
L-Cystine	C7602	0.2	240.3	48.1
L-Glutamine	49419	4	146.14	584.6
L-Histidine	53319	0.2	155.15	31.0
L-Isoleucine	W527602	0.8	131.17	104.9
L-Leucine	61819	0.8	131.17	104.9
L-Lysine	L9037	0.8	164.2	131.4
L-Methionine	64319	0.2	149.21	29.8
L-Phenylalanine	P5482	0.4	165.19	66.1
L-Serine	S4311	0.4	105.09	42.0
L-Threonine	89179	0.8	119.12	95.3
L-Tryptophan	93659	0.08	204.23	16.3
L-Tyrosine	93829	0.4	181.19	72.5
L-Valine	V0513	0.8	117.15	93.7
Vitamin				
Choline citrate	C2004	0.03	295.29	8.9
D-calcium pantothenate	P5155	0.008	238.27	1.9
Folic acid	F8758	0.009	441.4	4.0
Niacinamide	PHR1033	0.033	122.12	4.0
Pyridoxine (neutral)	P5669	0.02	169.18	3.4
Riboflavin	R4500	0.001	376.36	0.4
Thiamine ntrate	CDS000474	0.012	327.36	3.9
Myoinositol	57569	0.04	180.16	7.2
Bulk salts/minerals				
Sodium glutanate	S2054	115	218.14	25.08
Sodium bicarbonate	S5761	44	84.007	3,696.3
Calcium lactate	L4388	1.8	218.22	392.8
Iron (III) Nitrate	254223	0.001	404	0.4
Magnesium sulfate	M9397	0.8	246.47	197.2
Sodium phosphate monobasic	71492	0.4	119.98	48.0
Sodium phospahte dibasic	71629	0.3	141.96	42.6
D-Glucose	G7021	25	180.16	4,504.0
Sodium pyruvate	P2256	1	110.04	110.0
Antibiotic				
Penicillin P3032	P3032	100 U/ml	356.3	60.45
Streptomycin S1277	S1277	100 U/ml	728.69	100

Reference

Wallace, A.C., R.A. Laskowski, and J.M. Thornton. 1995. LIGPLOT: a program to generate schematic diagrams of protein-ligand interactions. *Protein Eng.* 8:127–134. http://dx.doi.org/10.1093/protein/8.2.127